Electronic Supplementary Material (ESI) for Physical Chemistry Chemical Physics.

Supplementary Materials

Hydrogen Abstraction/Addition Reactions in Soot Surface Growth

Qingzhao Chu[1,2], Baolu Shi[2], Hongyu Wang[1], Dongping Chen[1]*, Lijuan Liao[3]*

[1]*State Key Lab of Explosion Science and Technology, Beijing Institute of Technology, Beijing, 100081, China*

[2]*School of Aerospace Engineering, Beijing Institute of Technology, Beijing, 100081, China*

[3] *Key Laboratory for Mechanics in Fluid Solid Coupling Systems, Institute of Mechanics, Chinese Academy of Sciences, Beijing, 100190, China*

In the supplementary material, we present:

- Methods: Fig. S1 to S7
- Results: Fig. S8 to S10
- Derivation of binary collision assumption for QCT method
- Derivation of collision radius from MD simulations

1. Methods

In this work, polycyclic aromatic hydrocarbons (PAH) stacks are used to construct the soot surface. Two parameters *d* and *h* are closely related to the potential energy of the target surface, where parameters *d* and *h* represent the layer separation and horizontal distance between the center of mass of neighboring PAH monomers. To grant the configurations at the minimum potential energy, the impact of parameters *d* and *h* on the potential energy surface are carefully examined in Fig. S1. Considering the two types of building block in this paper, *i.e.* A19-A19 and A7-A7, we found that the minimum of potential energy surface (PES) located at *d* = 3.3 Å (Fig. S1a), and *h* = 10.2 Å for A7-A7, *h* = 15.1 Å for A19-A19 (Fig. S1b).

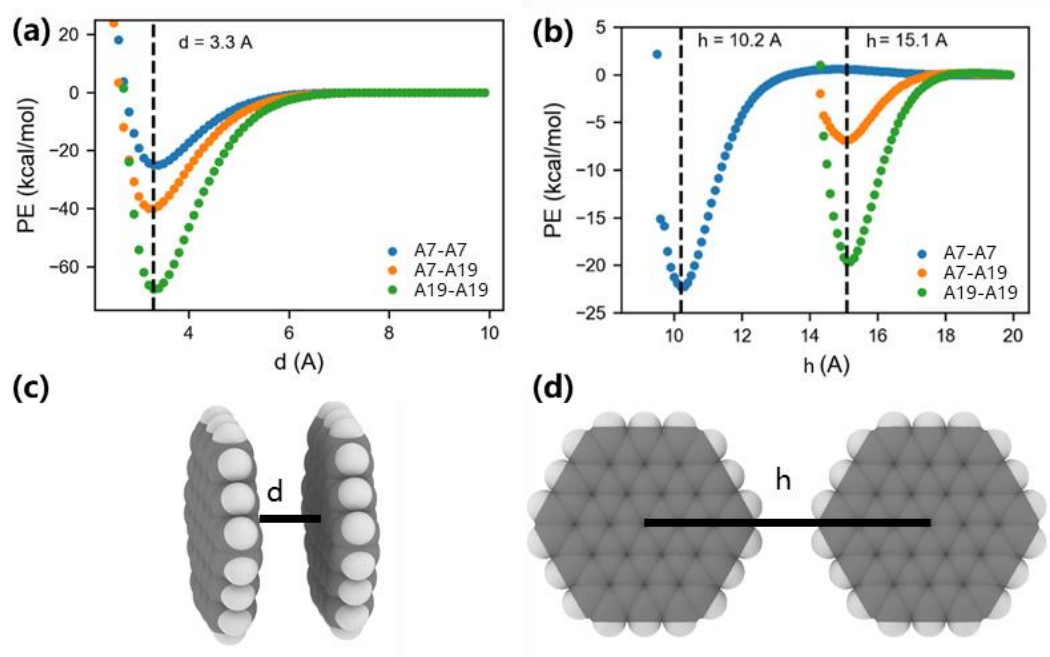

Figure S1. (a-b) Potential energy surface of A7-A7, A7-A19 and A19-A19 dimers. The illustrations of parameters *d* and *h* are listed in (c-d).

The bottom layer of the quasi-surface is restrained to avoid PAH evaporation. To investigate the effect of restrain on the reaction dynamics, we examined the kinetic energy transfer and reaction probability on the surface of A19 stacks with and without restrain. The kinetic energy transfer is examined by the average values of all of incident H atoms at inlet and outlet times, and a minor impact is observed (Fig. S2). Note that the kinetic energy at the inlet time refers to its initial kinetic energy, and the outlet

time is defined as the instance when the distance between H atom and the surface is larger than 20 Å. Also, the predictions of P_{HB} and P_{HD} are insensitive to the application of restrain.

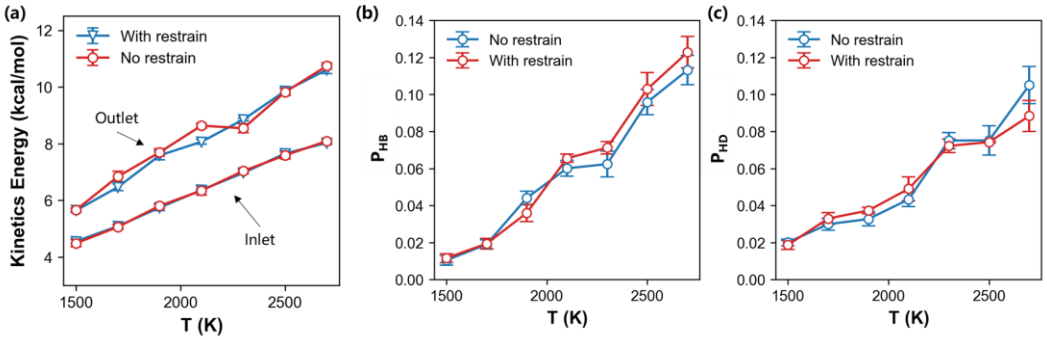

Figure S2. Featured properties in the collision dynamics between H atoms and A19s with and without restrains including (a) kinetic energy transfer, (b) the probability of HB reaction and (c) the probability of HD reaction.

The numerical convergences of reaction probabilities are investigated (Fig. S3). Two types of reactions are included, *i.e.* hydrogen abstraction (HB) and hydrogen addition (HD). All probabilities gradually converge as the sample numbers increase. The converged results require at least 6000 and 3000 runs for PAH monomers and quasi-surface, respectively.

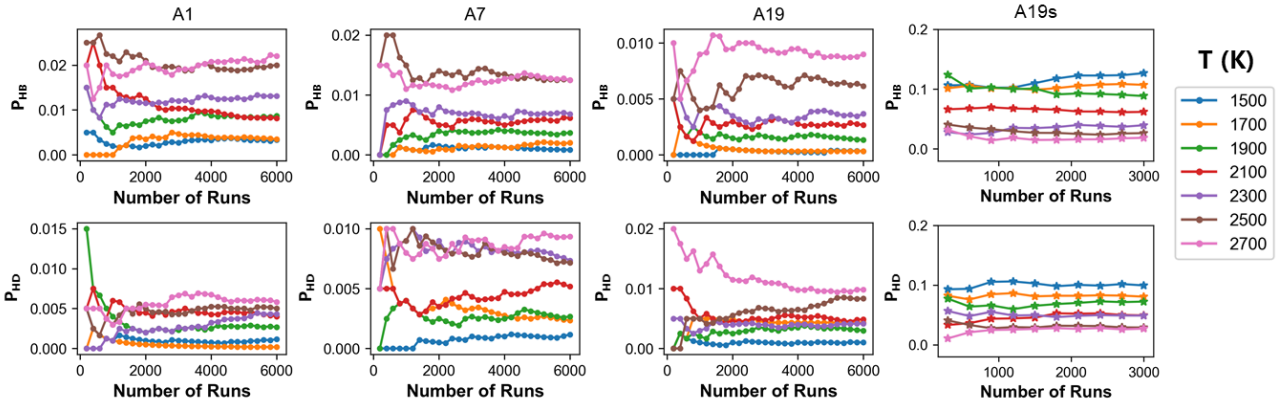

Figure S3. The numerical convergence of reaction probabilities in the cases of A1, A7, A19 and A19s.

An improper time step might lead to issues in the energy conservation. We performed a test simulation of an A19 molecule in the NVE ensemble using Δt = 0.1 and 0.2 fs. The initial velocity of atoms is assigned from the Maxwell-Boltzmann distribution at 2700 K. The evolution of per-atom total

energy is shown in Fig. S4. The deviation is negligible suggesting that a time step of 0.2 fs is sufficient for the energy conservation in this work.

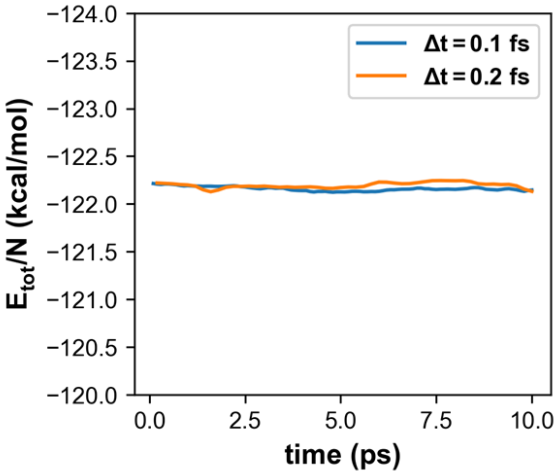

Figure S4. Total energy of an A19 molecule using two timesteps.

To validate the accuracy of force field for reactive events, the potential energies of reactants, transition state and products are calculated using B3LYP/6-31G*, M06-2X/6-311G** and ReaxFF, respectively. The structure of transition state (TS) is located using B3LYP/6-31G* level of theory. The energy barriers between reactants and TS structures are compared to illustrate the quality of the ReaxFF parameterization. The results are shown in Fig. S5, the energy barrier of ReaxFF are in line with the value by M06-2X/6-311G** (16.23 *vs.* 16.85 kcal/mol), and is better than that using B3LYP/6-31G* method.

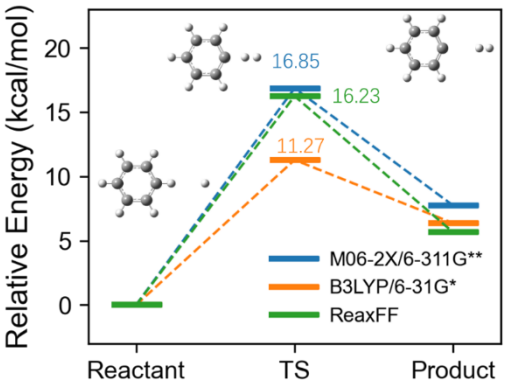

Fig. S5. Potential energy profiles for the reactant, transition state and product of hydrogen abstraction from benzene at M06-2X/6-311G**, and B3LYP/6-31G* level of theory, respectively. The corresponding values from ReaxFF forcefield are also marked for comparison.

The formation and breakage of chemical bonds are recognized by the atomic distance and duration. If the distance of two atoms, *i.e.* r, is shorter than the critical value r_{crit} and the duration exceeds t_{crit}, these two atoms are considered as bonded. To determine the critical values of r_{crit} and t_{crit} for both C-H and H-H bonds, we analyzed the trajectories of A1+H reactions in Fig. S6. For H-H bonds at 2700 K, if r_{crit} is too short (*e.g.* purple region), almost no bond can be recognized. If r_{crit} is too long (*e.g.* red region), the code will misinterpret the bond formation, and overestimate the bond number. For H-H bonds at 2700 K, the bond number remains unchanged for r_{crit} = 1.0-1.4 Å and t_{crit} = 0.2-0.4 ps. For H-H bonds at 1500 K, the results follow the same trend. Therefore, r_{crit} = 1.0 Å and t_{crit} = 0.2 ps are used to capture the reaction dynamics for H-H bond over the temperature range of 1500-2700 K. For C-H bond, values of r_{crit} = 1.2 Å and t_{crit} = 0.2 ps were adopted.

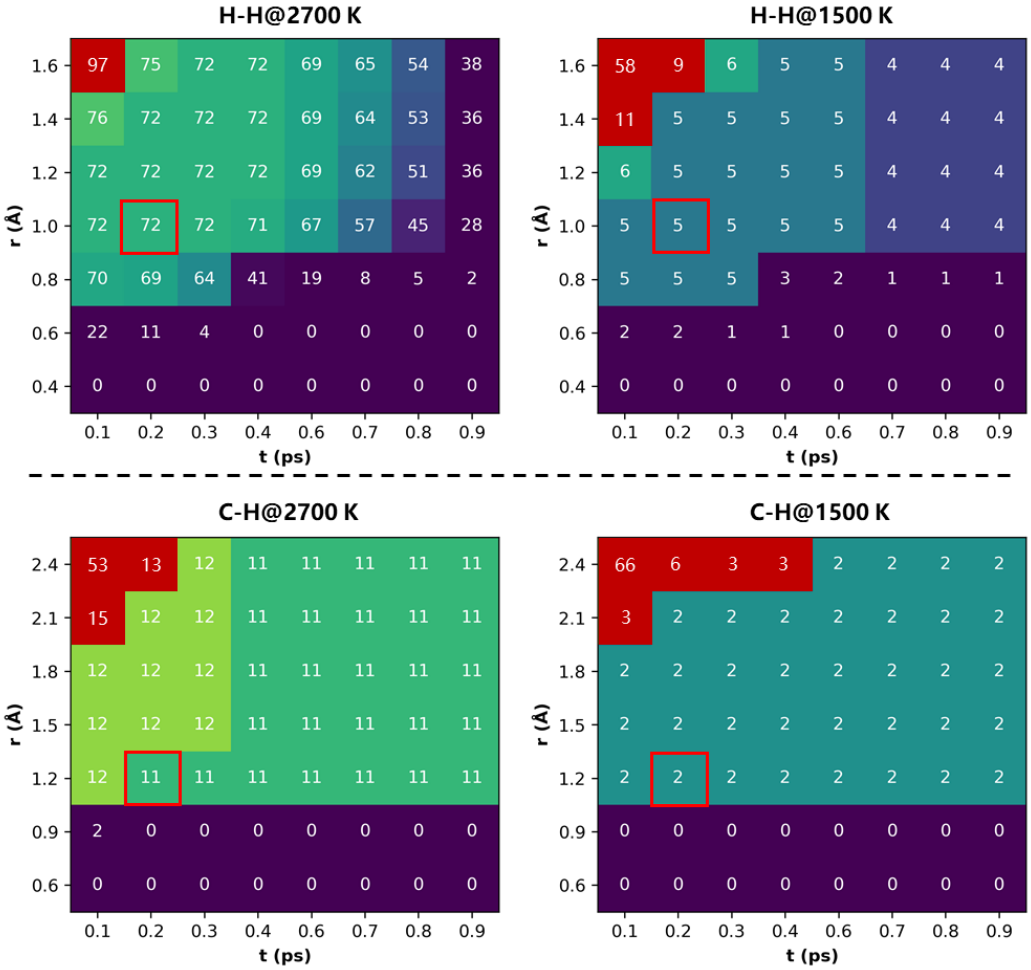

Figure S6. The bond numbers of H-H and C-H bonds with a critical distance r_{crit} and a time duration t_{crit} at 1500 and 2700 K. Every number in the lattice represents the number of recognized bonds over 3000 trajectories. The highlighted squares refer to bond information using the critical r_{crit} and t_{crit}.

The bootstrapping resampling method is used to estimate the error bars in our calculations. The effects of sample size and repeats on the HB reaction probabilities at 1500 and 2700 K are shown in Fig. S7. It is clear that the converged result can be extracted from a sample size and repeat number as 3000 and 20, respectively.

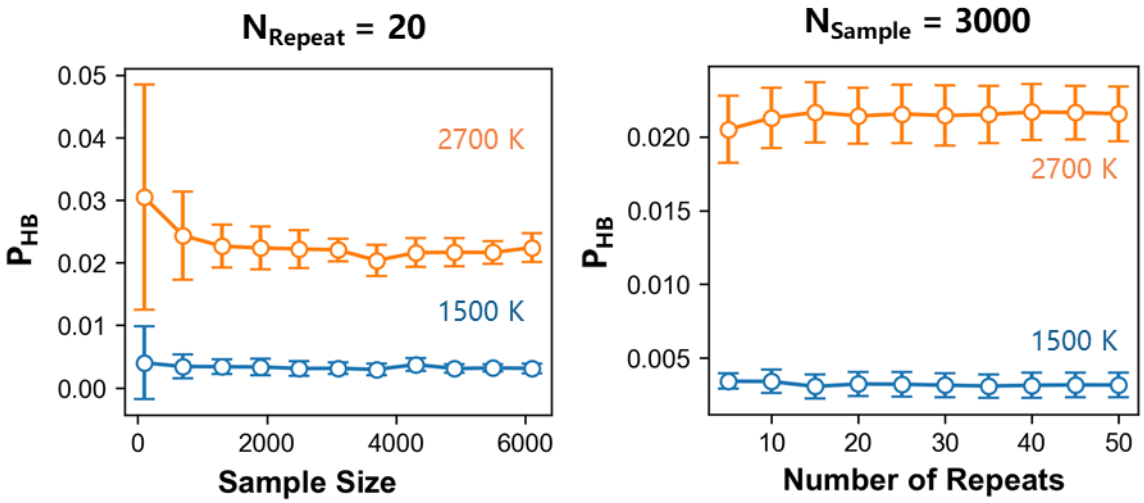

Figure S7. The HB reaction probability on A1 molecules at 1500 and 2700 K. The error bars are constructed from one standard derivation.

2. Results

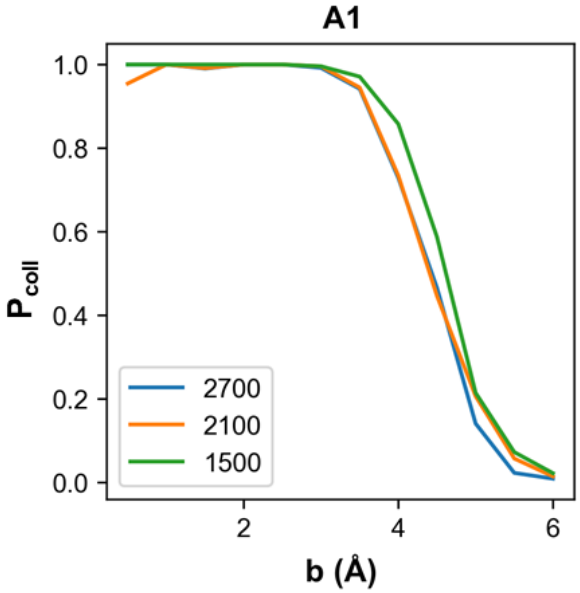

Figure S8. Collision probability between H atoms and A1 at 1500, 2100, and 2700 K.

The collision probabilities between H atoms and A1 at 1500, 2100, and 2700 K are shown in Fig. S8. The collision probability is almost 100% for b < 3 Å, and it starts to decay for larger b. No obvious temperature dependence is observed from 1500 to 2700 K, and this can be attributed to the weak van der Waals potential between the incident H atom and PAH molecules.

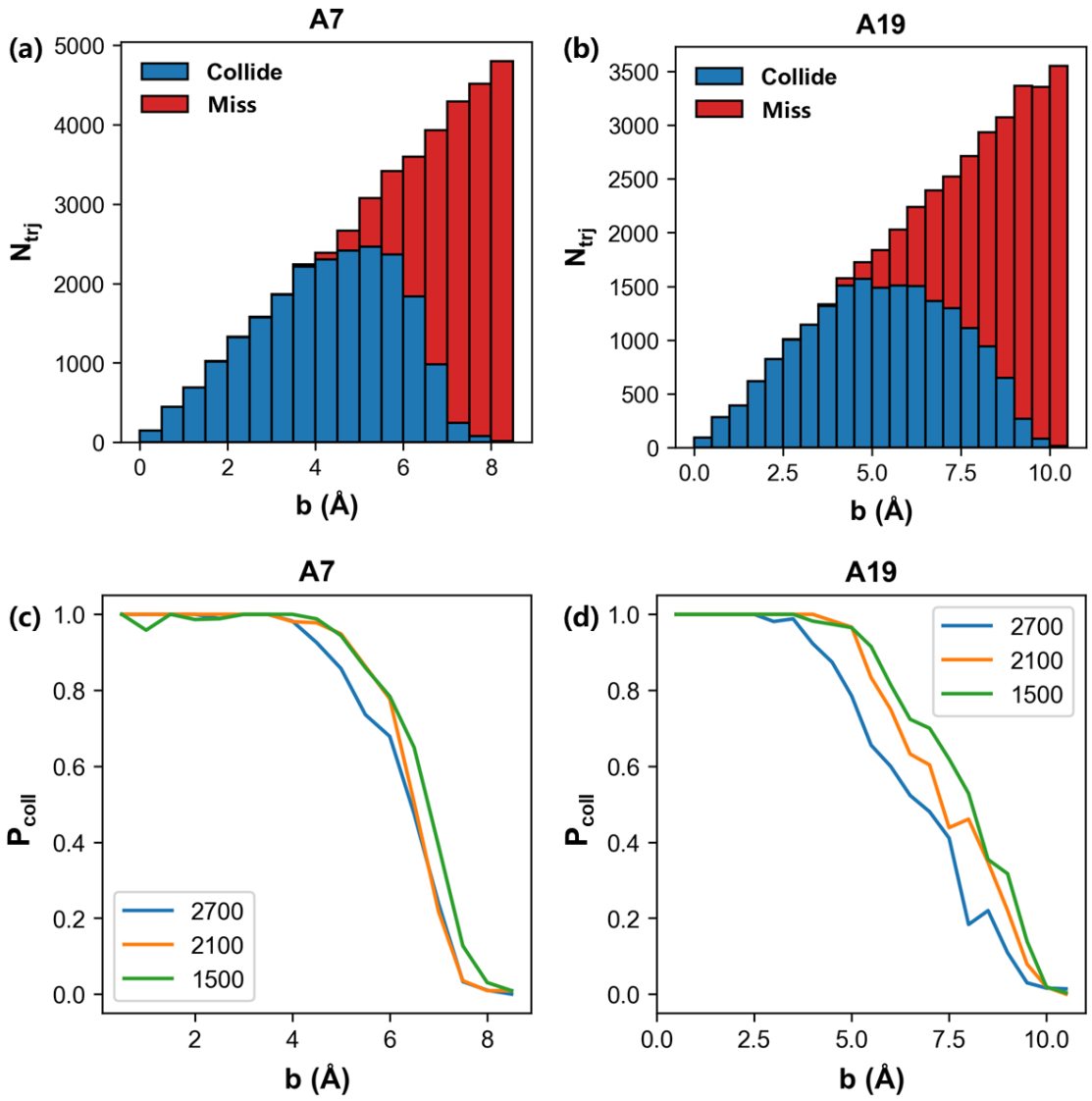

Figure S9. Distribution of impact factor for collision and missed trajectories for (a) A7 and (b) A19. Probability of collision as a function of impact factor at T = 1500, 2100, and 2700 K for (c) A7 and (d) A19.

The collision dynamics of A7 and A19 monomer with an incident H are similar to A1 molecule. As Fig. S9 shows, the collision probability is 1 for b < 3 Å, while it decreases to 0 for larger impact factors. For both cases, the predicted collision probabilities are insensitive to the temperature from 1500 to 2700 K.

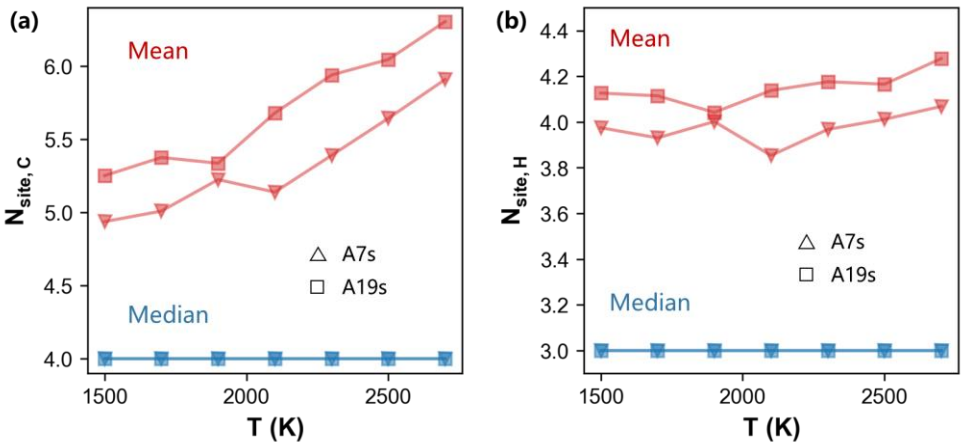

Figure S10. The mean and median of the numbers of collision events occurring on (a) C and (b) H sites in a single trajectory of A7s and A19s.

The mean and median values of both $N_{site,C}$ and $N_{site,H}$ are presented in Fig. S10. It is found that the median values are insensitive to the change in the temperature. The mean values of $N_{site,H}$ are also independent on the temperature, while the number of $N_{site,C}$ increases by one on average as temperature changes from 1500 to 2700 K. Overall, we notice that both $N_{site,C}$ and $N_{site,H}$ has a weak dependence on the temperature.

3. Derivation of binary collision assumption for QCT method

In our case, we assume that the incident H atom does not interact with other species during the sampling time ($t = 10\ ps$). We can estimate the pressure (p) by following equations.

$$p = n\, k_b \frac{T}{N_A} \tag{S1}$$

$$n = \frac{1}{t\, S\, P_{site} \sqrt{\frac{8 k_b T}{\pi \mu}}} \tag{S2}$$

$$P_{site} = \frac{S_{site}}{S} \tag{S3}$$

where k_b is the Boltzmann constant, n is the number density, N_A is the Avogadro number, S and S_{site} are the collision cross-section area of total surface and specific reactive site, respectively. P_{site} is the probability that a third body collides with the same reactive site as the incident H atom, and μ is the effective mass. We can estimate the upper limit of pressure for the QCT methods using eqs. S1-S3.

Combining eqs. S1 and S2, we found that p is independent with S. For all the systems at 2000 K ($S_{site} = 18.1$ Å^2 for H site), the upper limit of pressure is 23.1 atm. If system pressure exceeds this critical value, the binary collision assumption fails, and the interactions between incident species should be considered.

4. The derivation of collision radius from MD simulations

For an impact factor b, we have the collision probability $P_{coll}(b)$, and the collision cross section in the range of b and $(b + db)$ can be written as

$$dA_c = \text{area} \times \text{probability of collision} = (2\pi b\ db) \times P_{coll}(b) \quad \text{(S4)}$$

By integrating eq. (S4) over $(0, b_{max,sample})$, we have

$$A_c = \int_0^{b_{max,sample}} 2\pi b P_{coll}(b) db \quad \text{(S5)}$$

The collision radius can be written as

$$R_{c,MD} = \left(\frac{A_c}{\pi}\right)^{\frac{1}{2}} = \left(\int_0^{b_{max,sample}} 2b\ P_{coll}(b) db\right)^{\frac{1}{2}} \quad \text{(S6)}$$